Automatic Microaneurysm Detection from Non-dilated Diabetic Retinopathy Retinal Images Using Mathematical Morphology Methods

Akara Sopharak, Bunyarit Uyyanonvara and Sarah Barman

***Abstract*— To develop an automated diabetic retinopathy screening system, a detection of lesions in digital fundus photographs is needed. Microaneurysms are the first clinical sign of diabetic retinopathy. The number of microaneurysms is used to indicate the severity of the disease. Early microaneurysm detection can help reduce the incidence of blindness. This paper investigates a set of optimally adjusted morphological operators used for microaneurysm detection on non-dilated pupil and low-contrast retinal images. The detected microaneurysms are validated by comparing with ophthalmologists' hand-drawn ground-truth. As a result, the sensitivity, specificity, precision and accuracy were 81.61, 99.99, 63.76 and 99.98%, respectively.**

***Index Terms*— diabetic retinopathy, microaneurysms, mathematical morphology.**

I. Introduction

Diabetic retinopathy (DR) is the commonest cause of blindness in people of working age. The global prevalence of diabetes is expected to rise to 4.4% of the global population by 2030 [1]. An effective treatment to prevent vision loss is available, but diabetic retinopathyis asymptomatic until late in the disease process. The screening of diabetic patients for the development of diabetic retinopathy can reduce the risk of blindness by 50% [2]-[4]. With a large number of patients, the number of ophthalmologists is not sufficient to cope with all patients, especially in rural areas or if the workload of local ophthalmologists is substantial. The damage caused by DR can be prevented if it is treated in early stages. Therefore, automated early detection could limit the severity of the disease and assist ophthalmologists in investigating and treating the disease more efficiently.

The appearance of microaneurysms (MA), haemorrhages and exudates would represent the degree of DR. MA are focal dilations of retinal capillaries and appear as small round dark red dots as shown in Fig. 1(a) and 1(b). Haemorrhages occur when blood leaks from the retinal vessels and appear as round small red dots or blots indistinguishable from MA. Exudates are proteins or lipids leak from blood vessel and appear as yellowish color. It isdifficult to detect MA because their pixels are similar to that of blood vessels. MA is hard to distinguish from noise or background variations because it has typically low contrast. In this paper we concentrate on MA detection as the earliest clinically localized characteristic of DR [5]. Their detection can be used to grade the DR stage into four stages: no DR, mild DR, moderate DR, and severe DR as shown in Table 1 [6].

A number of methods for MA detection have been published. T. Spencer et al. [7], M.J. Cree et al. [8] and A. Frame et al. [9] propose a mathematical morphology technique to segment MA within fluorescein angiograms. J.H. Hipwell et al. [10] use Gaussian matched filters to retain candidate MA for classification. Gardner et al. [11] use a back propagation neural network on sub-images (20x20 or 30x30 pixel windows). C. Sinthanayothin et al. [12] propose an automated system of detection of diabetic retinopathy using recursive region growing segmentation (RRGS). D. Usher et al. [13] employ a combination of RRGS and adaptive intensity thresholding to detect candidate lesion regions and a neural network is used for classification. T. Walter et al. [14] propose a method based on diameter closing and kernel density estimation for automatic classification. B. Dupas et al. [6] use a diameter-closing to segment MA candidate regions and k-nearest neighbours (*k*NN) to classify MA. M. Niemeijer et al. [15] combine prior works by T. Spencer et al. [7] and A. Frame et al. [8] with a detection system based on pixel classification and new features are proposed. A *k*NN classifier was used in the final step. B. Zhang et al. [16] use multi-scale correlation coefficients (MSCF). They detect coarse MA candidate using MSCF and fine MA using features classification.

Most techniques mention earlier work on fluorescein angiographies or color images taken on patients with dilated pupils in which the MA and other retinal features are clearly visible. The examination time and effect on the patient could be reduced if the detection system could succeed on images taken from patients with non-dilated pupils. However, the quality of these images will be worse and it greatly affects the performance of those mentioned algorithms.

A. Sopharak is with Faculty of Science and Arts, Burapha University, Chanthaburi Campus, 57 Moo 1, Kamong, Thamai, Chantaburi 22170, Thailand (phone: +66(0)39-310-000; e-mail: akara@buu.ac.th).

B. Uyyanonvara is with Sirindhorn International Institue of Technology, Thammasat University, 131 Moo 5, Tiwanont Road, Bangkadi, Muang, Pathumthani, 12000, Thailand (e-mail: bunyarit@siit.tu.ac.th).

S. A. Barman is with Kingston University, Penrhyn Road, Kingston Upon Thames, Surrey, KT1 2EE, United Kingdom (e-mail : S.Barman@kingston.ac.uk).

Automatic MA detection on images acquired without pupil dilation is investigated in this work with the aim of providing decision support in addition to reducing the workload of ophthalmologists.

In our previous work, we have presented methods for automatic exudate detection using a mathematical morphological technique, a FCM clustering technique, a combination of FCM and mathematical morphology, a naive Bayesian classifier, a SVMs classifier and a nearest neighbor classifier [17]-[20]. A preliminary MA detection system is published [21]. To improve the overall ability of DR detection system, a MA detection method is proposed.

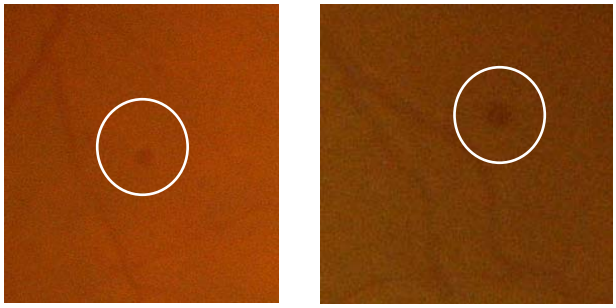

(a) (b)

Fig. 1. (a) and (b) Retinal image containing microaneurysms.

TABLE I
CRITERIA USED FOR GRADING DIABETIC RETINOPATHY

DR stage	
Grade 0 (no DR)	MA = 0 and H =0
Grade 1 (mild)	1≤ MA ≤ 5 and H =0
Grade 2 (moderate)	5< MA < 15 or 0< H ≤ 5
Grade 3 (severe)	MA ≥ 15 or H > 5

MA = microaneurysm, H = haemorrhage

II. METHOD

All digital retinal images taken from patients with non-dilated pupils were obtained from a KOWA-7 non-mydriatic retinal camera with a 45° field of view. The image size is 752 x 500 pixels with 24 bits per pixel.

The proposed system has three main steps. The preprocessing step includes noise removal, contrast enhancement and shade correction. Candidate retinal features which may cause a false detection, i.e., exudates and vessels are detected in the second step. And the last step is MA detection by using a set of optimally adjusted mathematical morphology. The overall procedure of MA detection is shown in Fig. 2.

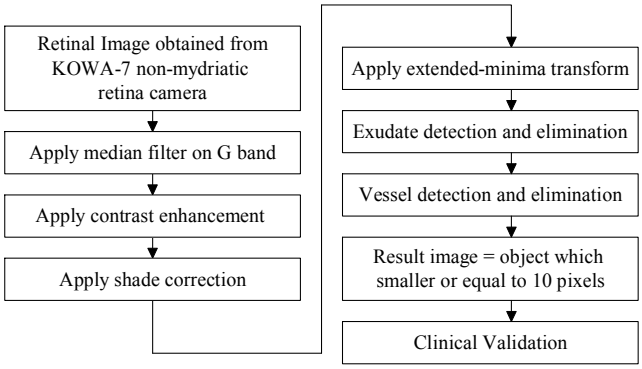

Fig. 2. Procedure of microaneurysm detection.

A. Preprocessing

Retinal images used in this experiment have poor contrast, noise and non-uniform illumination. A preprocessing step is needed to improve the image quality prior to the detection step. The green plane (f_g) of the original image in RGB plane is used as red lesions such as MA and blood vessels have the highest contrast with the background in this color plane [22]. This is shown in Fig.3, which represents image in original RGB image, red plane, green plane and blue plane, respectively. A median filtering operation is applied on f_g to attenuate the noise before a Contrast Limited Adaptive Histogram Equalization was applied for contrast enhancement. A dark region (including noise and MAs) may dominate after contrast enhancement. To account for this a shade correction algorithm is applied to the green band in order to remove slow background variation due to non-uniform illumination. An illumination variation involves only low spatial frequencies. A shade corrected image is accomplished by subtracting the image with a low pass filter, in this experiment, the result of a 35x35 median filter applied to the image to correct for background variation.

The green band image after removal of noise and contrast enhancement, and the shade corrected image (f_{sc}) are shown in Fig. 4 (a) and 4 (b). Closeups MA are shown in Fig. 5 (a) through Fig. 5 (d).

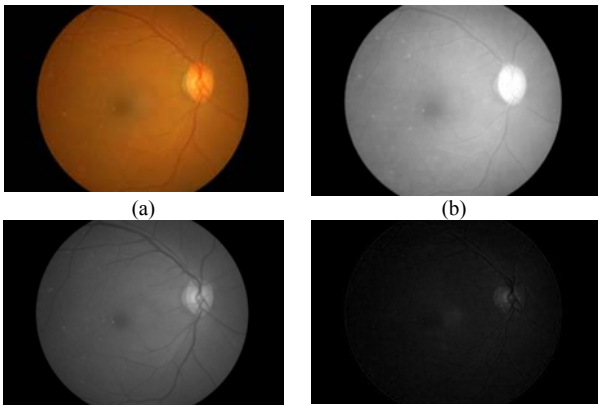

(a) (b)

(c) (d)

Fig. 3. Retinal images. (a) Original RGB plane (b) red plane (c) green plane (d) blue plane.

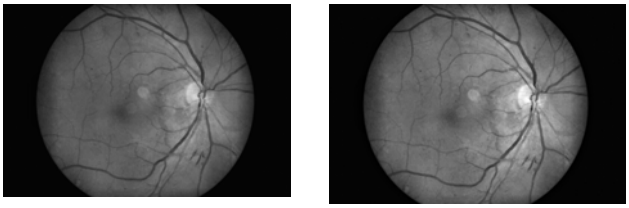

(a) (b)

Fig. 4. Preprocessing steps. (a) Green band after contrast enhancement (b) Shade corrected image.

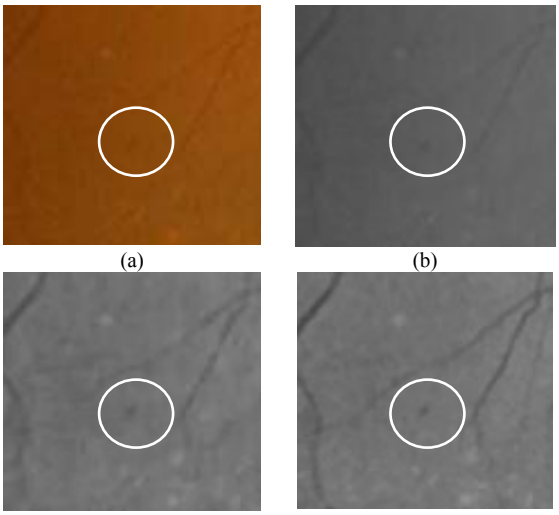

(a) (b) (c) (d)

Fig. 5. Closeups of microaneurysm (a) Original RGB Image. (b) Green band. (c) Green band after contrast enhancement. (d) Shade corrected image.

B. Exudate Detection

MA detection is our main purpose, however we have to remove bright lesions such as exudates prior to the process because when they lie close together, small islands are formed between them and they can be wrongly detected as MAs. Mathematical morphological methods (proposed in our previous work [16]) was used due to its computationally low cost. High contrast vessels are first eliminated from intensity image, and then the resulting image is thresholded. Morphological reconstruction is used for exudate detection. Examples of exudate detection results overlaid on the original image are shown in Fig. 6.

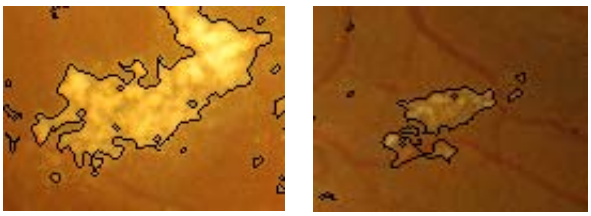

Fig. 6. Exudate detection results shown overlaid on original images.

C. Vessel Detection

Vessels are another element in the image that needs to be removed prior the MA detection since MA and vessels both appear in a reddish color and MAs cannot occur on vessels. They appear as isolated patterns and disconnected from the vessels.

To detect vessels, two intermediate images are generated. The first image is obtained using a closing operator (ϕ) on the shade corrected image (f_{sc}) to eliminate the details and dark patterns (vessels) from the image. A flat disc-shaped structuring element with a fixed radius of ten (B_1) is used. A second image is obtained by filled-in small black dots on the shade corrected image (f_{sc}) with diameters smaller than size of MA in order to remove small red objects and fill holes in the vessel. The diameter of a MA lies between 10 and 100 μm, but it always smaller then a diameter $\lambda < 125$ μm [6]. In our image set of size 752 x 500 pixels, the size of a MA is about 10 pixels. Vessel candidate areas are obtained by the difference between the first image and the second image from the previous step. The closing image and filled in image are shown in Fig. 7 (a) and Fig. 7 (b).

$$f_{vesselDiff} = \phi^{(B_1)}(f_{sc}) - fill(f_{sc}) \quad (1)$$

where B_1 is the morphological structuring element.

The candidate vessels are then binarized by thresholding at grey level α_1 as in (2). Let $T = \{t_{min},\ldots,t_{max}\}$ be an ordered set of grey levels, we have

$$f_{vesselT} = T_{[\alpha_1, t_{\max}]}(f_{vesselDiff}) \quad (2)$$

As a result shown in Fig. 7 (c), there are some small isolated objects left. The objects which have size smaller than 10 pixels (size of MA, as mentioned above) are then removed from $f_{vesselT}$. The result is shown in Fig. 7 (d).

D. Microaneurysm Detection

Retinal MAs are focal dilatations of retinal capillaries. They are discrete, localized saccular distensions of the weakened capillary walls and appear as small round dark red dots on the retinal surface.

According to the medical definition of MA [5], [6], it is a reddish, circular pattern with a diameter $\lambda < 125$ μm. We aim to find an MA by its diameter and isolated connected red pixels with a constant intensity value, and whose external boundary pixels all have a higher value; in the green plane of a RGB image.

A preprocessed retinal image is used as preliminary image for MA detection. The extended-minima transform is the regional minima of h-minima transform [23]. It is applied to the f_{sc} image. This transformation is a thresholding technique that brings most of the valleys to zero. The h-minima transform suppresses all the minima in the intensity image whose depth is less than or equal to a predefined threshold. The output image f_E is a binary image with the white pixels represent the regional minima in the original image. Regional minima are connected pixels with the same intensity value, whose external boundary pixels all have a higher value. The output is a binary image. The extended minima transform on the f_{sc} image with threshold value α_2 is shown in (3).

$$f_E = EM(f_{sc}, \alpha_2) \quad (3)$$

where f_E is the output image.

The selection of threshold is very important where the higher value of α_2 will lower the number of regions and a

lower value of α_2 will raise the number of regions. The result is shown in Fig. 7 (e). A slight change in threshold value can cause the method either over-segment or under-segment the MA. The previous detected exudates and vessels were removed from the resulting image. The result is shown in Fig. 7 (f).

$$f_{VE\_removed} = f_E - f_{vesselT} - f_{ex} \quad (4)$$

where f_{ex} is the exudate detected image.

Then the objects with a size smaller or equal to 10 pixels are selected and classified as MAs. The result is shown in Fig. 7 (g).

There are parameters used in this experiment. They are, namely, the size of structuring element (B_1) used for the closing operation, threshold values (α_1 and α_2,). α_1 was calculated automatically using the Otsu algorithm. B_1 and α_2 were varied and tested in order to assess the algorithm performance in an experiment. Each parameter was varied as follows:

$B_1 \in \{7, 9, 10, 11, 12\}$
$\alpha_2 \in \{0.01, 0.03, 0.05, 0.07, 0.09\}$

All parameters in this proposed method are set using the values that gave highest sensitivity and specificity in the previous experiment. The experiment showed that the value of B_1=10 and α_2 = 0.05 gave a good balance between the number of detected MAs and the number of detected spurious objects.

III. Results

Data sets of 45 non-dilated retinal images are tested on an AMD Athlon 1.25 GHz PC using the MATLAB program. Each image took approximately 6 minutes to process (included exudates detection). Detected MAs are compared with the ophthalmologists' hand-drawn ground-truth images for verification. In order to facilitate the experts to produce a ground-truth image, a first draft of ground-truth image is created by us. We marked the very obvious MA pixels which are normally red dot areas, pixel by pixel, using a photo manipulation program with one colour. Then, this first draft image is shown to two expert ophthalmologists together with the original image. The ophthalmologists then made some changes by adding some missing MA pixels and/or removing some misunderstood non-MA pixels until it is agreed by both experts.

Sensitivity, specificity, precision and accuracy are chosen as measurement of the accuracy of the algorithms. All measures can be calculated based on four values, namely the true positive (TP) rate, the false positive (FP) rate, the false negative (FN) rate, and the true negative (TN) rate. These values are defined in Table 2. Sensitivity is the percentage of the actual MA pixels that are detected, and specificity is the percentage of non-MA pixels that are correctly classified as non-MA pixels. Precision is the percentage of detected pixels that are actually MAs. Accuracy is the overall per-pixel success rate of the classifier. The sensitivity, sensitivity, precision and accuracy are computed using (5) though (8), respectively.

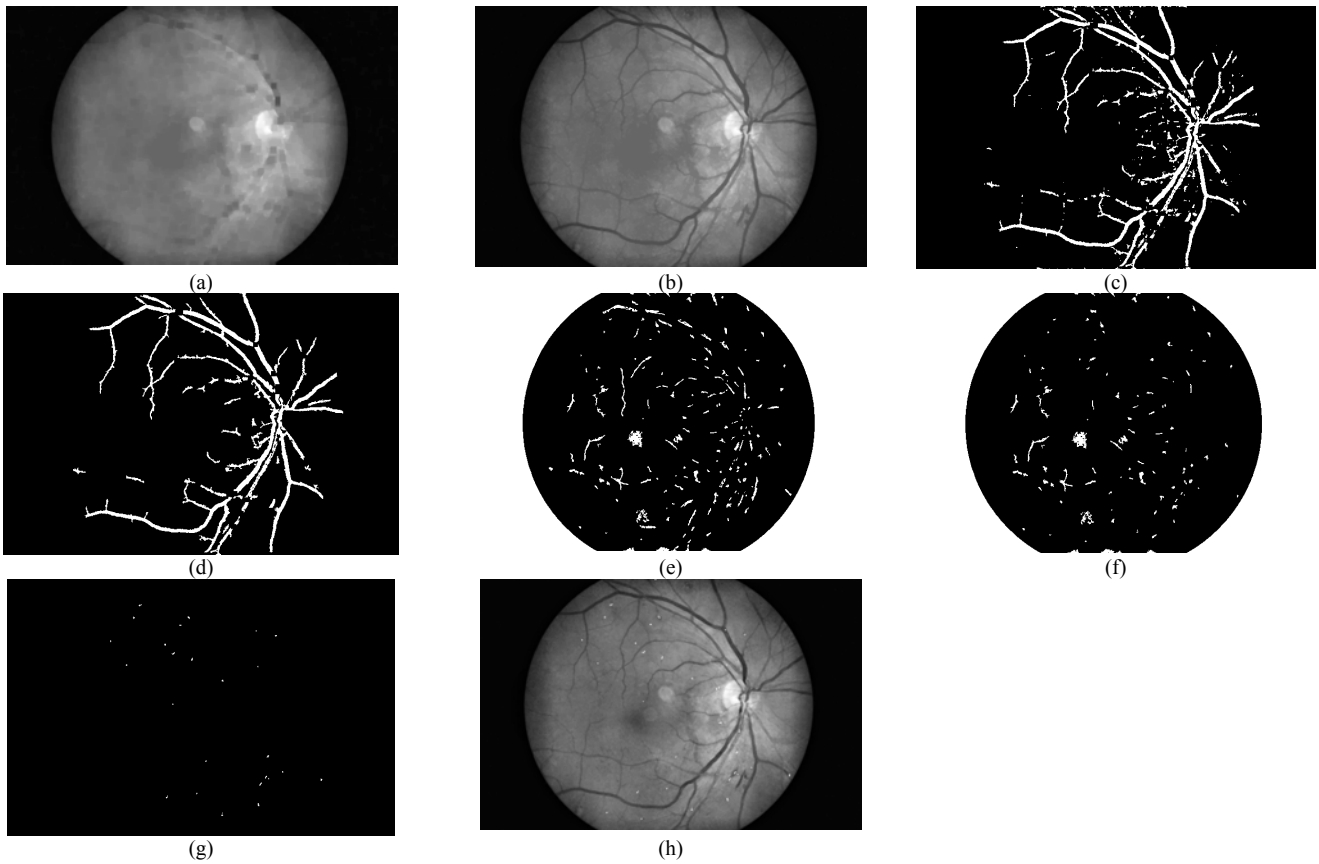

Fig. 7. Microaneurysm detection (a) Image after closing (b) Filled-in image (c) Difference image (d) Image after removal of object smaller than the size of microaneurysm from image (c) (e) Extended-minima transform image (f) Image after removal of vessels (g) Detected microaneurysms (h) Microaneurysms superimposed on original image.

TABLE II
PIXEL BASED EVALUATION

Test Result	Disease Status	
	Present	Absent
Positive	True Positive (TP)	False Positive (FP)
Negative	False Negative (FN)	True Negative (TN)

$$Sensitivity = \frac{TP}{TP + FN} \quad (5)$$

$$Specificity = \frac{TN}{TN + FP} \quad (6)$$

$$Precision = \frac{TP}{TP + FP} \quad (7)$$

$$Accuracy = \frac{TP + TN}{TP + FP + FN + TN} \quad (8)$$

Sensitivity, specificity, precision and accuracy in this experiment are 81.61, 99.99, 63.76 and99.98%, respectively. The numbers of MAs are also counted for automated grading of the severity of the DR. Example resulting images of MA detection are shown in Fig. 8.

VI. Conclusion and Discussion

Our work concentrates on microaneurysm detection from diabetic retinopathy patient's non-dilated pupil digital images. It is an extension to our previously proposed automated DR screening system. The system intends to help the ophthalmologists in the diabetic retinopathy screening process to detect symptoms faster and more easily. The algorithm could detect MAs on very poor quality images.

There are some incorrect MA detections which are caused by the artifacts, too small MA, too blurred MA, faint blood vessels which cannot detected/removed or MA that appear very faint. There are some missing MAs located next to or nearby blood vessels which are removed as wrongly detected as blood vessels. They are also faint blood vessels which are not removed in vessel detection step; MA could be wrongly detected on those vessels. For example, as shown in Fig.9 faint blood vessels can be incorrectly detected as MA. The results of MA detection depend on the success of vessel detection. A main weakness of the algorithm arises from the fact that the algorithm depends on vessel detection. This indicates the further necessity of improving the robustness of this task. Hemorrhages detection could be also added to the system in order to increase its ability to verify the degree of diabetic retinopathy.

Although further development of this algorithm is still required, the results are satisfying. The outcome is quite successful with sensitivity and specificity of 81.61% and 99.99%, respectively. The system also provided ophthalmologists with the number of MAs for grading the DR stage. In order to apply to a clinical application, the proposed method will be combined with an exudate detection system.

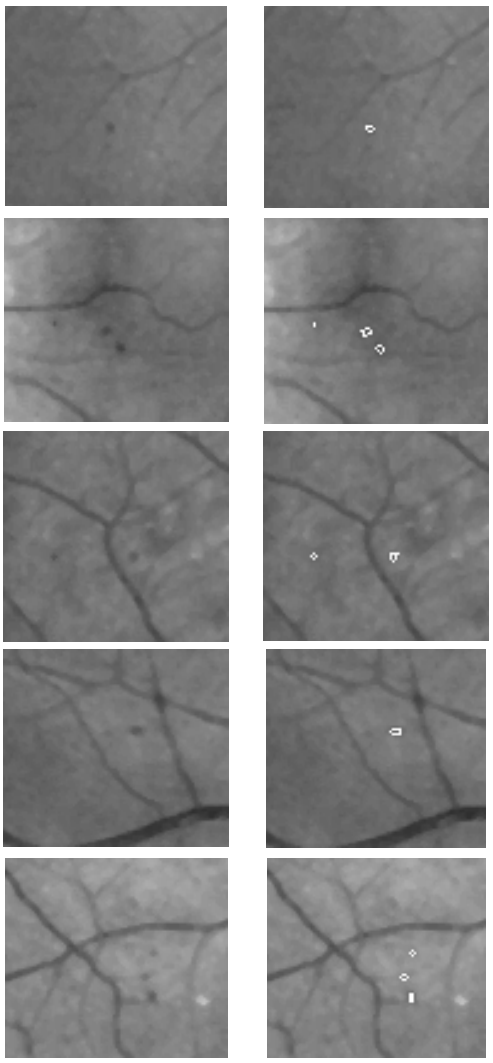

(a) (b)

Fig. 8. Example of microaneurysm detection results. (a) Original images. (b) Detected results.

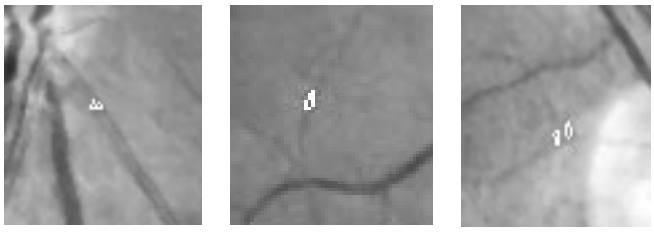

Fig. 9. Example of false microaneurysm detection on faint blood vessels.

Acknowledgment

This research is funded by the Burapha University, Chanthaburi Campus and National Research University Project of Thailand Office of Higher Education Commission (Thammasat University).

References

[1] S. Wild, G. Roglic, A. Green et al., "Global prevalence of diabetes: estimates for the year 2000 and projections for 2030," *Diabetes Care* 27, 2004, pp.1047-1053.

[2] W. Hsu, P.M.D.S Pallawala, Mong Li Lee et al., "The Role of Domain Knowledge in the Detection ofRetinal Hard Exudates," In *Proceedings of the 2001 IEEE Computer Society Conference on Computer Vision and Pattern Recognition* 2, 2001, pp.II-246 - II-251.

[3] A. Osareh, M. Mirmehdi, B. Thomas and R. Markham, "Automated Identification of Diabetic Retinal Exudates in Digital Colour Images," *British Journal of Ophthalmology* 87(10), 2003, pp.1220-1223.

[4] C.I. Sanchez, R. Hornero, M.I. Lopez et al., "Retinal Image Analysis to Detect and Quantify Lesions Associated with Diabetic Retinopathy," In *Proceedings of 26th IEEE Annual International Conference on Engineering in Medicine and Biology Society (EMBC)* 1, 2004, pp.1624 – 1627.

[5] P. Massin, A. Erginay, and A. Gaudric, "Retinopathie Diabetique", Elsevier, Editions scientifiques of m edicales, Elsevier, SAS, Paris 2000.

[6] B. Dupas, T. Walter, A. Erginay et al., "Evaluation of autom ated fundus photograph analysis algorithms for detecting microaneurysms, haemorrhages and exudates, and of a com puter-assisted diagnostic system for grading diabetic retinopathy," *Diabetes & Metabolism* 36(3), 2010, pp. 213-220.

[7] T. Spencer, J.A. Olson, K.C. McHardy et al., " An image-processingstrategy for the se gmentation and quantification of microaneurysms in fluor escein angiograms of the ocular fundus," *Comp Biomed Res* 29, 1996, pp. 284–302.

[8] M.J. Cree, J.A. Olso n, K.C. McHard y et al., "A fully automated comparative microaneurysm digital detection system," *Eye* 11, 1997, pp. 622–628.

[9] A. Frame, P. Undrill, M. Cree et al., "A comparison of computer based classification methods applied to th e detection of m icroaneurysms in ophthalmic fluorescein angiograms," *Comput. Biol. Med.* 28, 1998, pp. 225–238.

[10] J.H. Hipwell, F. Strachan, J.A. Olson et al., "Automated detection of microaneurysms in digital red-free photographs: a diabetic retinopathy screening tool," *Diabetic Medicine* 17, 2000, pp.588–594.

[11] G. Gardner, D. Keating, T.H. Williamson et al., " Automatic detection of diabetic retinopathy using an ar tificial neural network: a screening tool," *Br J Ophthalmol* 80, 1996, pp.940–944.

[12] C. Sinthanayothin, J.F. Boyce, T.H William son, T.H. et al., "Automated Detection of Diabe tic Retinopathy on Digital Fundus Image," *Diabetic Medicine* 19(2), 2002, pp. 105–112, 2002.

[13] D. Usher, M. Dumskyj, M. Himaga et al., "Automated Detection of Diabetic Retinopathy in Digital Retin al Images: A Tool for Diabetic Retinopathy Screening," *Diabetic Medicine* 21(1), 2004, pp. 84–90.

[14] T. Walter, P. Massin, A. Erginay et al., "Automatic detection of microaneurysms in color fundus im ages," *Medical Image Analysis* 11(6), 2007, pp.555-566.

[15] M. Niemeijer, B. van Ginneken, J. Staal et al., "Automatic detection of red lesions in digital color fundus photogr aphs," *IEEE Trans Med Imaging* 24(5), 2005, pp.584-592.

[16] B. Zhang, X. Wu, J. You et al., "Detection of microaneurysms using multi-scale correlation coefficients," *Pattern Recognition* 43(6), 2010, pp. 2237-2248.

[17] A. Sopharak, B. Uyyanonvara, S. Barman et al., "Automatic detection of diabetic retinopathy exudates from non-dilated retinal images using mathematical morphology methods," *Computer Medical Imaging and Graphics* 32(8), 2008, pp. 720-727.

[18] A. Sopharak, B. Uyyanonvara, and S. Barman, "Automatic exudate detection from non-dilated diabetic retinopathy retinal images using fuzzy C-means clustering," *Sensors* 9(3), 2009, pp. 2148-2161.

[19] A. Sopharak, M. Dailey, B. Uyyanonvara et al., "Machine Learning Approach to Autom atic Exudate Detection in Retinal I mages from Diabetic Patients," *Journal of Modern Optics* 57(2), 2010, pp. 124 – 135.

[20] A. Sopharak, B. Uyyanonvara, S. Barman et al., "Comparative Analysis of Automatic Exudate Detection Algorithms," In *Proceedings of the International Conference on Signal and Image Engineering (ICSIE)*, 2010, pp.738-741.

[21] A Sopharak, B Uy yanonvara, S Bar man et al., "Automatic Microaneurysm Detection from Non-dilated Diabetic Retinopathy Retinal Images," *Lecture Notes in Engineering and Computer Science: Proceedings of The World Congress on Engineering*, 2011, WCE 2011, 6-8 July, 2011, London, U.K., pp 1583-1586.

[22] Hoover, V.Kouznetsova, and M.Goldbaum, "Locating blood vessels in retinal images by piecewise thres hold probing of a m atched fileter response," IEEE Trans. Med. Imag. 19(3), 2000, pp. 203-210.

[23] P. Soille, Morphological Image Analysis: Principles and Applications, Springer-Verlag, 1999, pp. 170-171.

TABLE III
THE MICROANEURYSMS DETECTION RESULTS OF DISEASED RETINAL IMAGES

24 bit images	TP	TN	FP	FN	Sensitivity (%)	Specificity (%)	Precision (%)	Accuracy (%)
Image1	51	4	4	375941	92.73	100.00	92.73	99.99
Image2	56	7	0	375937	100.00	100.00	88.89	99.99
Image3	60	6	0	375934	100.00	100.00	90.91	99.98
Image4	38	40	15	375907	71.70	99.99	48.72	99.99
Image5	181	143	23	375653	88.73	99.96	55.86	99.95
Image6	127	64	6	375803	95.49	99.98	66.49	99.96
Image7	65	110	8	375817	89.04	99.97	37.14	99.98
Image8	39	10	0	375951	100.00	100.00	79.59	99.99
Image9	275	28	39	375658	87.58	99.99	90.76	99.92
Image10	25	82	0	375893	100.00	99.98	23.36	99.99
Image11	120	0	6	375874	95.24	100.00	100.00	99.97
Image12	9	23	8	375960	52.94	99.99	28.13	100.00
Image13	28	41	12	375919	70.00	99.99	40.58	99.99
Image14	57	26	14	375903	80.28	99.99	68.67	99.98
Image15	51	0	18	375931	73.91	100.00	100.00	99.98
Image16	77	49	25	375849	75.49	99.99	61.11	99.97
Image17	19	122	13	375846	59.38	99.97	13.48	99.99
Image18	44	9	6	375941	88.00	100.00	83.02	99.99
Image19	31	142	4	375823	88.57	99.96	17.92	99.99
Image20	38	25	2	375935	95.00	99.99	60.32	99.99
Image21	31	0	30	375939	50.82	100.00	100.00	99.98
Image22	72	49	9	375870	88.89	99.99	59.50	99.98
Image23	48	70	10	375872	82.76	99.98	40.68	99.98
Image24	77	17	9	375897	89.53	100.00	81.91	99.98
Image25	48	45	27	375880	64.00	99.99	51.61	99.98
Image26	37	195	20	375748	64.91	99.95	15.95	99.98
Image27	57	110	12	375821	82.61	99.97	34.13	99.98
Image28	53	20	28	375899	65.43	99.99	72.60.	99.98
Image29	81	142	30	375747	72.97	99.96	36.32	99.97
Image30	76	56	0	375868	100.00	99.99	57.58	99.98
Image31	159	73	44	375724	78.33	99.98	68.53	99.95
Image32	40	25	31	375904	56.34	99.99	61.54	99.98
Image33	216	95	14	375675	93.91	99.97	69.45	99.94
Image34	255	102	24	375619	91.40	99.97	71.43	99.93
Image35	139	90	15	375756	90.26	99.98	60.70	99.96
Image36	123	22	0	375855	100.00	99.99	84.83	99.97
Image37	7	2	6	375985	53.85	100.00	77.78	100.00
Image38	19	0	0	375981	100.00	100.00	100.00	99.99
Image39	14	5	5	375976	73.68	100.00	73.68	99.99
Image40	99	20	15	375866	86.84	99.99	83.19	99.97
Image41	128	69	6	375797	95.52	99.98	64.97	99.96
Image42	79	40	12	375869	86.81	99.99	66.39	99.98
Image43	65	43	30	375862	68.42	99.99	60.19	99.97
Image44	35	19	36	375910	49.30	99.99	64.81	99.98
Image45	38	40	15	375907	71.70	99.99	48.72	99.99
	AVERAGE				81.61	99.99	63.76	99.98